RESEARCH ARTICLE OPEN ACCESS

Distinctive Pattern of Metal Deposition in Neurologic Wilson Disease

Insights From 7T Susceptibility-Weighted Imaging

Dongning Su, MD, PhD,* Zhijin Zhang, BS,* Zhe Zhang, PhD,* Sujun Zheng, MD, PhD, Tingyan Yao, BS, Yi Dong, MD, PhD, Wanlin Zhu, PhD, Ning Wei, PhD, Yue Suo, MD, PhD, Xinyao Liu, BS, Huiqing Zhao, MD, PhD, Zhan Wang, MD, PhD, Huizi Ma, MD, PhD, Wei Li, MD, PhD, Junhong Zhou, PhD, Joyce S.T. Lam, MSc, Tao Wu, MD, PhD, Petr Dusek, MD, A. Jon Stoessl, MD, Xiaoping Wang, MD, PhD, Jing Jing, MD, PhD, and Tao Feng, MD, PhD

Neurology® 2024;102:e209478. doi:10.1212/WNL.0000000000209478

Correspondence
Dr. Feng
bxbkyjs@sina.com
or Dr. Wang
x_p_wang@sjtu.edu.cn
or Dr. Jing
jingj_bjttyy@163.com

Abstract

Background and Objectives

Noninvasive and accurate biomarkers of neurologic Wilson disease (NWD), a rare inherited disorder, could reduce diagnostic error or delay. Excessive subcortical metal deposition seen on susceptibility imaging has suggested a characteristic pattern in NWD. With submillimeter spatial resolution and increased contrast, 7T susceptibility-weighted imaging (SWI) may enable better visualization of metal deposition in NWD. In this study, we sought to identify a distinctive metal deposition pattern in NWD using 7T SWI and investigate its diagnostic value and underlying pathophysiologic mechanism.

Methods

Patients with WD, healthy participants with monoallelic *ATP7B* variant(s) on a single chromosome, and health controls (HCs) were recruited. NWD and non-NWD (nNWD) were defined according to the presence or absence of neurologic symptoms during investigation. Patients with other diseases with comparable clinical or imaging manifestations, including early-onset Parkinson disease (EOPD), multiple system atrophy (MSA), progressive supranuclear palsy (PSP), and neurodegeneration with brain iron accumulation (NBIA), were additionally recruited and assessed for exploratory comparative analysis. All participants underwent 7T T1, T2, and high-resolution SWI scanning. Quantitative susceptibility mapping and principal component analysis were performed to illustrate metal distribution.

Results

We identified a linear signal intensity change consisting of a hyperintense strip at the lateral border of the globus pallidus in patients with NWD. We termed this feature "hyperintense globus pallidus rim sign." This feature was detected in 38 of 41 patients with NWD and was negative in all 31 nNWD patients, 15 patients with EOPD, 30 patients with MSA, 15 patients with PSP, and 12 patients with NBIA; 22 monoallelic *ATP7B* variant carriers; and 41 HC. Its sensitivity to differentiate between NWD and HC was 92.7%, and specificity was 100%. Severity of the hyperintense globus pallidus rim sign measured by a semiquantitative scale was positively

MORE ONLINE

Class of Evidence
Criteria for rating therapeutic and diagnostic studies
NPub.org/coe

*These authors contributed equally to this work as co-first authors.

From the Department of Neurology (D.S., Zhijin Zhang, H.Z., Z.W., H.M., W.L., T.W., J.J., T.F.), Beijing Tiantan Hospital, Capital Medical University; China National Clinical Research Center for Neurological Diseases (D.S., Zhijin Zhang, Zhe Zhang, W.Z., N.W., Y.S., X.L., H.Z., Z.W., H.M., W.L., T.W., J.J., T.F.); Tiantan Neuroimaging Center of Excellence (Zhe Zhang, W.Z., N.W., Y.S., X.L., J.J.), and Department of Hepatology (S.Z.), Beijing Youan Hospital, Capital Medical University; Department of Neurology (T.Y.), Xuanwu Hospital, Capital Medical University, National Clinical Research Center for Geriatric Disorders; Senior Department of Hepatology (Y.D.), the Fifth Medical Center of PLA General Hospital, Beijing, China; Hinda and Arthur Marcus Institute for Aging Research (J.Z.), Hebrew SeniorLife, Roslindale; Harvard Medical School (J.Z.), Boston, MA; Pacific Parkinson's Research Centre (J.S.T.L., A.J.S.), Djavad Mowafaghian Centre for Brain Health, University of British Columbia, Vancouver, Canada; Department of Neurology and Centre of Clinical Neuroscience (P.D.), First Faculty of Medicine, Charles University and General University Hospital, Prague, Czech Republic; Division of Neurology (A.J.S.), Department of Medicine, University of British Columbia, Vancouver, Canada; and Department of Neurology (X.W.), Jiading Branch of Shanghai General Hospital, Shanghai Jiao Tong University School of Medicine, China.

Go to Neurology.org/N for full disclosures. Funding information and disclosures deemed relevant by the authors, if any, are provided at the end of the article.

The Article Processing Charge was funded by the authors.

Glossary

AIC = Akaike information criterion; **EOPD** = early-onset Parkinson disease; **GAS** = Global Assessment Scale; **HC** = healthy control; **MPAN** = mitochondrial membrane protein-associated neurodegeneration; **MSA** = multiple system atrophy; **MSA-C** = MSA-cerebellar type; **MSA-P** = MSA-parkinsonian type; **NBIA** = neurodegeneration with brain iron accumulation; **NWD** = neurologic WD; **nNWD** = non-NWD; **PCA** = principal component analysis; **PKAN** = pantothenate kinase-associated neurodegeneration; **PLAN** = phospholipase A2-associated neurodegeneration; **PSP** = progressive supranuclear palsy; **QSM** = quantitative susceptibility mapping; **SWI** = susceptibility-weighted imaging; **UWDRS** = Unified Wilson's Disease Rating Scale; **WD** = Wilson disease.

correlated with neurologic severity (ρ = 0.682, 95% CI 0.467–0.821, $p < 0.001$). Patients with NWD showed increased susceptibility in the lenticular nucleus with high regional weights in the lateral globus pallidus and medial putamen.

Discussion

The hyperintense globus pallidus rim sign showed high sensitivity and excellent specificity for diagnosis and differential diagnosis of NWD. It is related to a special metal deposition pattern in the lenticular nucleus in NWD and can be considered as a novel neuroimaging biomarker of NWD.

Classification of Evidence

The study provides Class II evidence that the hyperintense globus pallidus rim sign on 7T SWI MRI can accurately diagnose neurologic WD.

Introduction

Wilson disease (WD), also known as hepatolenticular degeneration, is a rare inherited autosomal recessive disorder caused by variants in *ATP7B*, leading to pathologic copper accumulation mainly in the liver and brain.[1] WD patients with neurologic manifestations such as parkinsonism, dysarthria, and postural tremor are classified as neurologic WD (NWD).[2-4] Early diagnosis of NWD is crucial because early treatment can prevent irreversible neurologic sequelae. However, delayed diagnosis of NWD is common[5,6] because its phenotypic manifestations often overlap with other neurologic disorders.

Although brain MRI is routinely included in the diagnostic approach of WD,[7] we still lack a neuroimaging feature with high sensitivity and specificity. Most patients with NWD show T2 hyperintensities in the basal ganglia, thalamus, and/or brainstem because both lenticular nucleus and tectal plate signal changes have been reported to be present in approximately 75% of patients with NWD.[8,9] Another recognized feature, "face of the giant panda" sign, was only observed in 14.3%–27.3% of patients with NWD.[9,10] These signal changes, however, have been reported in other metabolic diseases and infectious diseases.[11,12] Although WD is primarily characterized by an abnormal copper metabolism, postmortem studies have found excessive accumulation of both copper and iron in the putamen, caudate nucleus, and dentate nucleus.[13,14] MRI studies using susceptibility-weighted imaging (SWI), quantitative susceptibility mapping (QSM), and T2* sequences have also reported excessive metal deposition in the globus pallidus and putamen.[15-19] Nevertheless, clinical application of these quantitative sequences is currently limited by the lack of standardized scanning processes and quantitative parameters. Although pathologic studies have revealed different microscopic patterns of iron deposition in WD and other neurologic disorders,[20] it remains unclear as to whether the macroscopic metal deposition pattern of NWD, especially in the basal ganglia, is distinct from that observed in other diseases with brain metal accumulation.

With submillimeter spatial resolution and increased tissue contrast, susceptibility imaging in ultra-high-field 7T MRI is superior to 3 T MRI.[21,22] 7T MRI has proven to be a feasible tool in the visualization of the nigrosome 1[23] and the central vein sign,[24] both of which are useful in guiding disease diagnosis. Taken together, 7T SWI may be used to identify a distinctive pattern of metal deposition in NWD, which could increase the accuracy of NWD diagnosis. No such study has been conducted to date.

Using 7T MRI, we conducted a cross-sectional diagnostic study including patients with NWD, non-NWD (nNWD) patients, monoallelic *ATP7B* variant carriers, and healthy controls (HCs). We aim to identify a novel imaging feature, which related to the distinctive pattern of metal deposition of NWD, to accurately diagnose NWD. On successful identification, we investigated its diagnostic value and correlation with neurologic severity of NWD. In addition, we performed a preliminary exploratory analysis in patients with comparable clinical or imaging manifestations, including early-onset Parkinson disease (EOPD), multiple system atrophy (MSA),

progressive supranuclear palsy (PSP), and neurodegeneration with brain iron accumulation (NBIA),[25-27] to examine the specificity of this pattern of metal deposition. QSM and principal component analysis (PCA) were performed to illustrate the underlying pathophysiologic mechanism.

Methods

Participants

This study was conducted between May 2021 and June 2023. Participants were recruited from 2 movement disorder centers and 2 hepatology centers in China, with all assessments and scanning procedures being performed at Beijing Tiantan Hospital.

The inclusion criteria were (1) patients with WD: patients with diagnosis of WD according to the European Association for the Study of the Liver guidelines[7] with Leipzig score ≥4, genetic analysis showed at least 1 disease-causing *ATP7B* variant; (2) monoallelic *ATP7B* variant carriers: first-degree relatives (parents, siblings, and children) of WD patients with 1 or more disease-causing *ATP7B* variants on a single chromosome, and without hepatic, neurologic, or psychiatric disorders that may lead to the diagnosis of WD; (3) HC: healthy individuals verified by routine physical examination, age-matched and sex-matched with patients with WD; (4) other disease groups: patients with diagnosis of EOPD (age at onset before 40[25]), MSA, and PSP according to their respective clinical diagnostic criteria,[28-30] and patients with clinical evidence for NBIA and verified by genetic testing.[27] Details of the inclusion and exclusion criteria are presented in the eMethods.

Patients with WD were divided into 2 groups, the NWD group and the nNWD group, according to the presence or absence of neurologic dysfunction at the time of investigation.[2,3] Patients with NWD were further classified into different subgroups based on their clinical (active or stable) and treatment (drug-naive, non–drug-naive) status. According to a previous study active NWD was defined as the onset of neurologic symptom(s) or neurologic deterioration in the preceding 6 months, whereas drug-naive patients with NWD were defined as patients who had never been treated with chelating agents and zinc salts.[31]

All patients with WD and their first-degree relatives underwent laboratory and ophthalmic examinations, structured rating scales including the Global Assessment Scale (GAS) for WD[32] and the Unified Wilson's Disease Rating Scale (UWDRS),[33] and *ATP7B* variant analysis. Details of the clinical evaluation and *ATP7B* variant analysis can be found in the eMethods.

Standard Protocol Approvals, Registrations, and Patient Consents

This study was approved and supervised by the Institutional Review Board of Beijing Tiantan Hospital, Capital Medical University and was conducted in accordance with the Declaration of Helsinki. All participants and/or their guardians provided written informed consent.

MRI Data Acquisition

All participants underwent 7T with high-resolution SWI scanned with the following parameters: transverse scan, acquisition voxel = 0.3 × 0.3 × 1.2 mm^3, 104 slices, time to echo = 12 milliseconds, repetition time = 19 milliseconds, flip angle = 14°, acceleration factor = 3, and scan time = 6:47. The raw MRI k-space data of SWI were saved for quantitative analysis (details in the Image Postprocessing section). Other MRI scans included T1-weighted and T2-weighted imaging (details in the eMethods).

Image Evaluation

Following the neuroimaging evaluation of patients with WD, monoallelic *ATP7B* variant carriers, and HC, we identified a linear hyperintensity strip at the lateral border of the globus pallidus and a hypointense signal of the globus pallidus and putamen in patients with NWD on the SWI images. We termed this feature "hyperintense globus pallidus rim sign" (Figure 1A).

The presence of the hyperintense globus pallidus rim sign was defined as a linear pseudohyperintense signal at the lateral border of the globus pallidus due to the hypointense signal of the globus pallidus and putamen, observed in more than 50% of the length of the lateral border of the globus pallidus on at least 3 serial planes of axial SWI images, starting from the thalamus level above the red nucleus, substantia nigra, and subthalamic nucleus and moving rostrally.

The hyperintense globus pallidus rim sign was rated on both sides according to the following criteria: a score of 0 when hyperintensity of the lateral border of the globus pallidus is invisible; a score of 1 when hyperintensity of the lateral border of the globus pallidus is visible, along with an unclear or discontinuous boundary and a mild increase in the signal of the lateral border of the globus pallidus and internal border of the putamen; a score of 2 when the hyperintensity of the lateral border of the globus pallidus is visible, with a clear and continuous boundary and a profound increase in the signal of the lateral border of the globus pallidus and internal border of the putamen (Figure 1B). The hyperintense globus pallidus rim sign was considered positive with a score of 1 or above on either side of the basal ganglia.

We additionally evaluated the presence of T2/SWI hypointensity[34] to assess the metal deposition in the NWD, nNWD, monoallelic *ATP7B* variant carriers, EOPD, MSA, PSP, NBIA, and HC groups. Full evaluation criteria are included in the eMethods.

Two neurologists, both with more than 5 years of experience in brain MRI, independently determined the presence of the imaging features and the rating of the hyperintense globus pallidus rim sign. The targeted images were entered into a

Figure 1 Diagram and Scoring Criteria of the Hyperintense Globus Pallidus Rim Sign

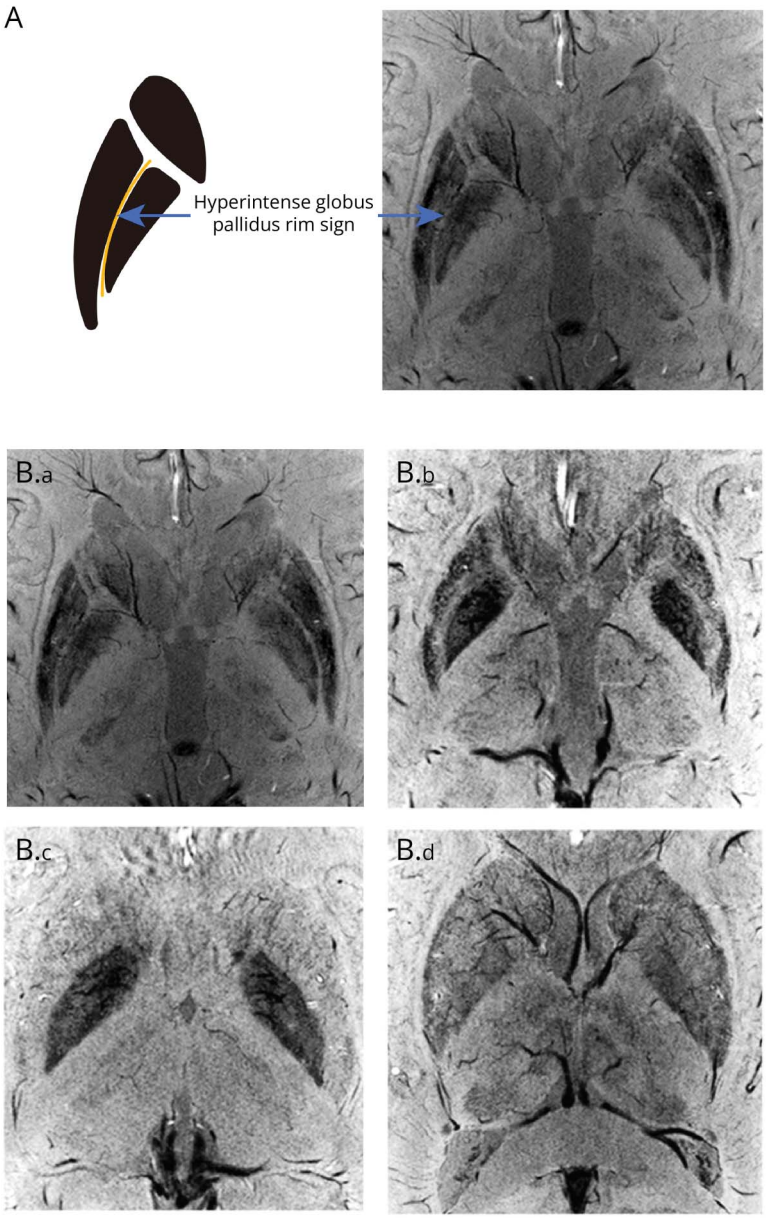

(A) A diagram of the hyperintense globus pallidus rim sign with a linear hyperintensity (arrow) at the lateral border of the globus pallidus and a hypointense signal of the globus pallidus and putamen on the axial SWI image of the basal ganglia. (B) Scoring criteria of the hyperintense globus pallidus rim sign show NWD patients with a score of 2 (B.a.) and a score of 1 (B.b.) on both sides, and HC (B.c.) and EOPD patient (B.d.) with a score of 0 on both sides. EOPD = early-onset Parkinson disease; HC = healthy control; NWD = neurologic Wilson disease; SWI = susceptibility-weighted imaging.

database and presented in anonymized and randomized manners, thereby ensuring that the 2 raters were blinded to the clinical diagnosis. For cases with inconsistent ratings, consensus decisions were achieved after discussion.

Image Postprocessing

As degeneration in the basal ganglia can lead to overlapping parkinsonian symptoms among patients with NWD, EOPD, MSA, and PSP, and increased susceptibility in the basal ganglia has been reported in these diseases,[25,26] we performed QSM analysis in the NWD, nNWD, EOPD, MSA, PSP, and HC groups.

QSM was reconstructed using the multiscale dipole inversion method from the single-echo gradient-echo data[35] in MATLAB (version R2020b; MathWorks, Natick, MA). The quantitative magnetic susceptibility (with the unit of parts per million) was extracted in the regions of interest including the globus pallidus and putamen. Voxel-wise PCA was performed on MNI-space QSM data. The comparisons were made between various disease groups (NWD, nNWD, EOPD, MSA, and PSP) and HC group, as well as between NWD group and MSA and PSP groups, respectively. Details of the QSM and PCA are shown in the eMethods.

Full image assessment procedures are presented in Figure 2.

Statistical Analysis

Statistical analysis was performed using SPSS (version 26.0; IBM, Chicago, IL). First, the Shapiro-Wilk test was used to

Figure 2 Flowchart of the Image Assessment Procedures

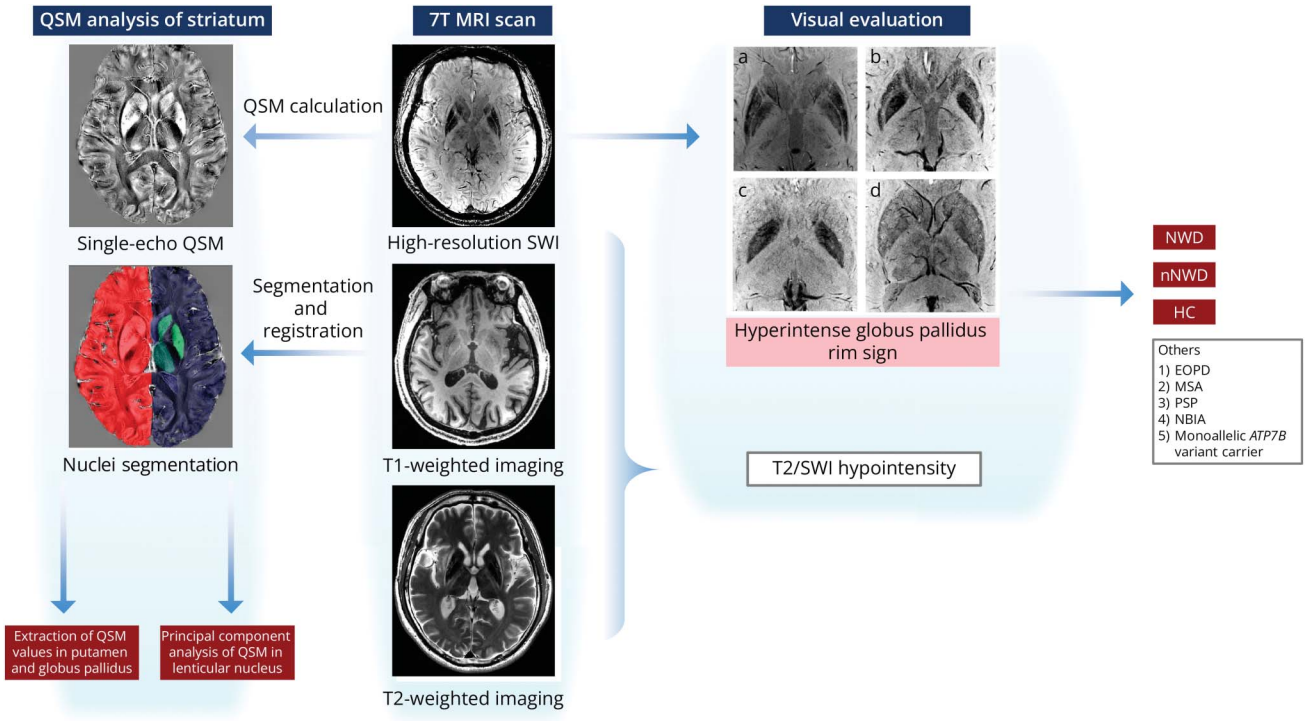

First, all participants underwent 7T MRI scanning including high-resolution SWI, T1, and T2 sequences. Second, a novel imaging feature, termed "hyperintense globus pallidus rim sign," was identified based on images obtained from patients with NWD, nNWD patients, monoallelic *ATP7B* variant carriers, and HC. This novel imaging feature was subsequently evaluated in other diseases, including EOPD, MSA, PSP, and NBIA. T2/SWI hypointensity was also assessed in the NWD, nNWD, monoallelic *ATP7B* variant carrier, HC, EOPD, MSA, PSP, and NBIA groups. Meanwhile, a semiquantitative scale was developed based on the severity of the hyperintense globus pallidus rim sign for correlation analysis. Finally, quantitative susceptibility mapping and principal component analysis of the putamen and globus pallidus were performed. EOPD = early-onset Parkinson disease; HC = healthy control; MSA = multiple system atrophy; NBIA = neurodegeneration with brain iron accumulation; NWD = neurologic Wilson disease; nNWD = nonneurologic Wilson disease; PSP = progressive supranuclear palsy; SWI = susceptibility-weighted imaging.

assess the normality of the continuous variables. Given the nonnormal distribution of the continuous variables, they are reported as median (interquartile range). The Mann-Whitney *U* test and Kruskal-Wallis test with Bonferroni correction for multiple comparisons were used for the 2-group analysis and the multigroup analysis, respectively. Categorical variables are presented as frequencies and percentages and were compared using the χ^2 test. Interobserver reliability was calculated using the Cohen κ coefficient and Kendall τ correlation coefficient for the identification of the imaging features (hyperintense globus pallidus rim sign and T2/SWI hypointensity) and the hyperintense globus pallidus rim sign scoring criteria, respectively. Diagnostic sensitivity, specificity, accuracy, positive predictive value, and negative predictive value were calculated according to the fourfold table. Correlation between the UWDRS scores and hyperintense globus pallidus rim sign scores was assessed using Spearman correlation. Owing to age-related increase[36] and treatment-related decrease[15] of iron deposition, age, disease duration, and treatment duration were then regressed out from the hyperintense globus pallidus rim sign scores, and the correlation between the residuals and UWDRS scores was further tested. The false discovery rate was used for multiple comparison correction. $p < 0.05$ was considered significant.

Data Availability

Anonymized data supporting the findings of this study are available from the corresponding author on reasonable request.

Results

Demographic and Clinical Characteristics

A total of 211 participants underwent MRI, with 2 patients with NWD, 1 monoallelic *ATP7B* variant carrier, and 1 HC excluded because of incomplete SWI acquisitions. A total of 207 participants, including 72 patients with WD (41 NWD patients, 31 nNWD patients), 22 monoallelic *ATP7B* variant carriers, 15 patients with EOPD, 30 patients with MSA (15 MSA-parkinsonian type [MSA-P], 15 MSA-cerebellar type [MSA-C]), 15 patients with PSP, 12 patients with NBIA, and 41 HC were included in the final analysis (eFigure 1).

The demographic and clinical measures of patients with WD and HC are presented in Table 1. No significant differences in age ($p = 0.533$) and sex ($p = 0.054$) were found among patients with NWD, nNWD patients, and HC. Patients with NWD had significantly lower Mini-Mental State Examination

Table 1 Demographic and Clinical Features of Patients With NWD, nNWD Patients, and HC

	NWD	nNWD	HC	*p* Value
n	41	31	41	—
Age, y	27.0 (21.0–34.0)	30.0 (22.0–37.0)	27.0 (24.0–36.5)	0.533[a]
Sex, male/female	30/11	14/17	24/17	0.054[b]
MMSE	29.0 (28.0–30.0)	30.0 (29.0–30.0)	30.0 (30.0–30.0)	<0.001[a]
Disease duration, y	3.0 (1.2–11.0)	3.0 (1.8–7.0)	—	0.918[c]
Treatment duration of chelating agents and/or zinc salts, y	1.2 (0.1–8.5)	1.5 (0.5–7.0)	—	0.968[c]
Treatment				
Chelating agents (D-penicillamine, dimercaptosuccinic acid)	27 (68.3)	21 (67.7)	—	0.866[b]
Zinc salts	26 (65.9)	19 (61.3)	—	0.854[b]
GAS for WD	13.0 (9.5–20.0)	4.0 (2.0–5.0)	—	<0.001[c]
UWDRS	16.0 (9.0–41.5)	0.0 (0.0–0.0)	—	<0.001[c]
Kayser-Fleischer ring	36 (87.8)	17 (54.8)	—	0.002[b]

Abbreviations: GAS for WD = Global Assessment Scale for Wilson disease; HC = healthy control; MMSE = Mini-Mental State Examination; NWD = neurologic Wilson disease; nNWD = nonneurologic Wilson disease; UWDRS = Unified Wilson's Disease Rating Scale.
[a] Kruskal-Wallis test.
[b] χ^2 test.
[c] Mann-Whitney *U* test.

scores compared with nNWD patients ($p = 0.02$) and HC ($p < 0.001$), with no significant difference between the NWD and nNWD groups ($p = 0.121$). Both NWD and nNWD groups had no significant differences in disease and anti-copper treatment duration ($p = 0.918$, $p = 0.968$). The demographic and clinical features of all participants are presented in eTables 1 and 2.

A total of 63 different *ATP7B* variants were detected in the 72 patients with WD and 22 monoallelic *ATP7B* variant carriers. The top 3 most common variants were c.2333G>T (27.9%), c.2975C>T (11.6%), and c.2621C>T (5.8%) in the NWD group, and c.2333G>T (21.0%), c.2621C>T (11.3%), c.2975C>T (6.5%), and c.3316G>A (6.5%) in the nNWD group. Frequencies of all identified *ATP7B* variants are listed in eTable 3.

Diagnostic Sensitivity and Specificity of the Hyperintense Globus Pallidus Rim Sign

The interrater reliability between observers was excellent for the identification of the hyperintense globus pallidus rim sign in the NWD, nNWD, monoallelic *ATP7B* variant carrier, EOPD, MSA-P, MSA-C, PSP, NBIA, and HC groups ($\kappa = 0.920$). The hyperintense globus pallidus rim sign was detected in 38 of the 41 patients with NWD and was absent in all the nNWD, EOPD, MSA-P, MSA-C, PSP, and NBIA patients; monoallelic *ATP7B* variant carriers; and HC (Figures 3 and 4). Detailed information of the 3 NWD patients with negative hyperintense globus pallidus rim sign is presented in eTable 4. The diagnostic sensitivity, specificity, accuracy, positive predictive value, and negative predictive value between patients with NWD and HC were 92.7%, 100.0%, 96.3%, 100%, and 93.2%, respectively. T2/SWI hypointensity was observed in 97.6% of patients with NWD, 19.4% of nNWD patients, 31.8% of monoallelic *ATP7B* variant carriers, 40% of patients with EOPD, 100% of patients with MSA-P, 93.3% of patients with MSA-C, 100% of patients with PSP, 91.7% of patients with NBIA and was absent in all HC ($\kappa = 0.919$). The differential diagnostic sensitivity of T2/SWI hypointensity between patients with NWD and EOPD was 97.6%, and the differential diagnostic specificity was 60%.

Analysis of Active vs Stable and Drug-Naive vs Non–Drug-Naive NWD Subgroups

Demographic, clinical, and imaging measures of NWD patient subgroups are presented in Table 2. The active NWD (n = 22) and drug-naive NWD (n = 10) groups had significantly shorter disease and treatment duration as well as significantly higher GAS for WD and UWDRS scores when compared with the stable NWD (n = 19) and non–drug-naive NWD groups (n = 31), respectively. The hyperintense globus pallidus rim sign was detected in all active patients with NWD and drug-naive patients with NWD, with diagnostic sensitivity, specificity, accuracy, positive predictive value, and negative predictive value all of 100%.

Scoring of the Hyperintense Globus Pallidus Rim Sign and Correlation Analysis in Patients With NWD

Scoring of the hyperintense globus pallidus rim sign showed high interrater reliability (Kendall τ b = 0.876). eTable 5

Figure 3 SWI Images of the Basal Ganglia in the NWD, nNWD, and HC Groups

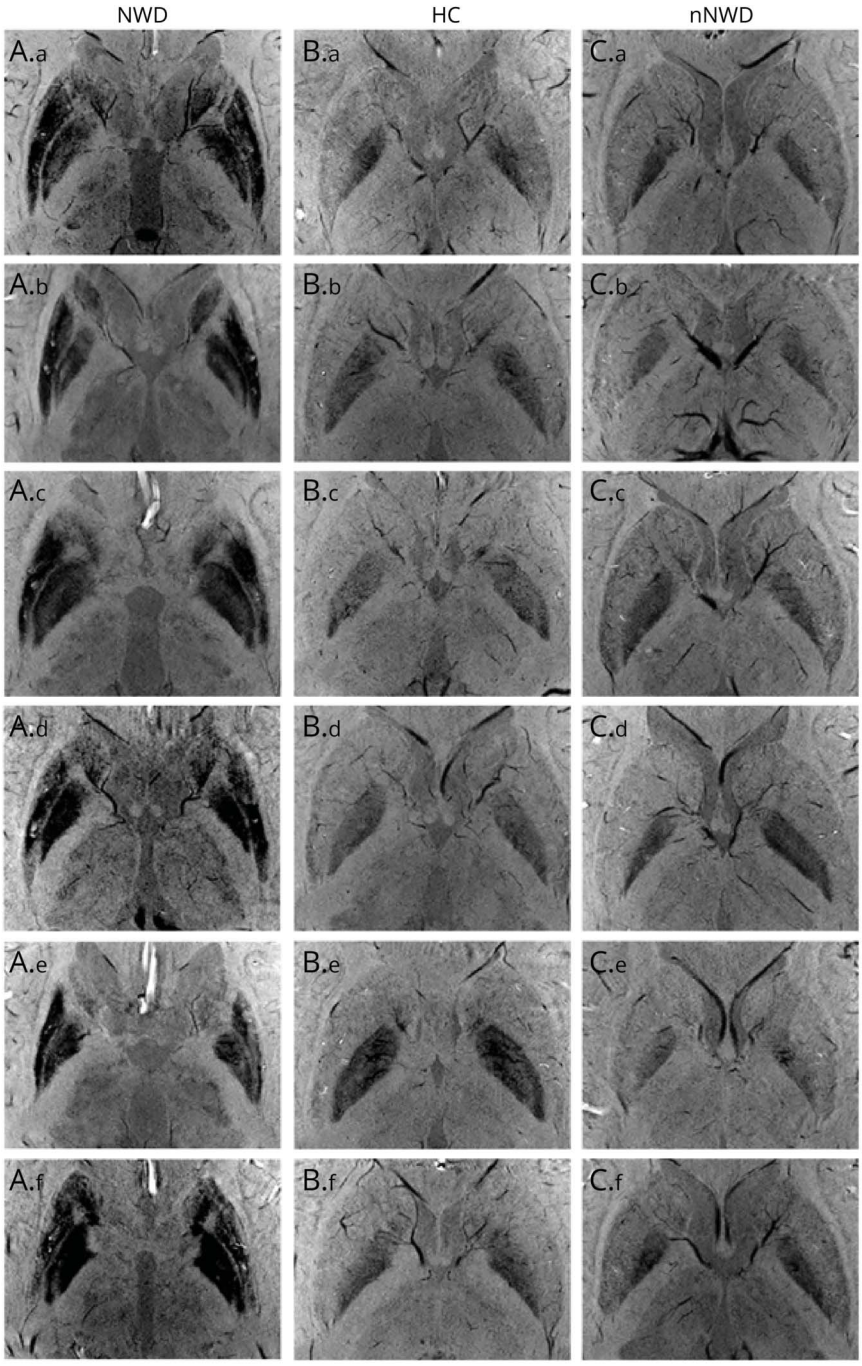

Axial 7T SWI images of the basal ganglia in typical patients with NWD (A.a.-A.f.), age-matched HC (B.a.-B.f.) and nNWD patients (C.a.-C.f.). The hyperintense globus pallidus rim sign is only observed in patients with NWD. HC = healthy control; NWD = neurologic Wilson disease; nNWD = nonneurologic Wilson disease; SWI = susceptibility-weighted imaging.

presents the distribution of the hyperintense globus pallidus rim sign score in patients with NWD. We established positive correlations between the hyperintense globus pallidus rim sign scores and the UWDRS scores in the NWD group (ρ = 0.682, 95% CI 0.467–0.821, $p < 0.001$) and in the NWD subgroups (ρ = 0.556, 95% CI 0.177–0.802, $p = 0.006$ in the active NWD group; ρ = 0.563, 95% CI 0.132–0.815, $p = 0.012$ in the stable NWD group; ρ = 0.756, 95% CI 0.221–0.941, $p = 0.011$ in the drug-naive NWD group; ρ = 0.639, 95% CI 0.358–0.814, $p < 0.001$ in the non–drug-naive NWD group). Following regression of age, disease duration, and treatment duration, positive correlations were found between the hyperintense globus pallidus rim sign scores and the UWDRS scores in the NWD group (ρ = 0.874, 95% CI 0.770–0.932, $p < 0.001$) and in the NWD subgroups (ρ = 0.918, 95% CI 0.804–0.967, $p < 0.001$ in the active NWD group; ρ = 0.635, 95% CI 0.240–0.849, $p = 0.004$ in the stable NWD group; ρ = 0.964, 95% CI 0.843–0.992 $p < 0.001$ in the drug-naive NWD group; ρ = 0.803, 95% CI 0.621–0.903, $p < 0.001$ in the non–drug-naive NWD group) (eFigure 2).

Figure 4 SWI Images of the Basal Ganglia in the Monoallelic *ATP7B* Variant Carriers, EOPD, MSA-P, MSA-C, PSP, and NBIA Groups

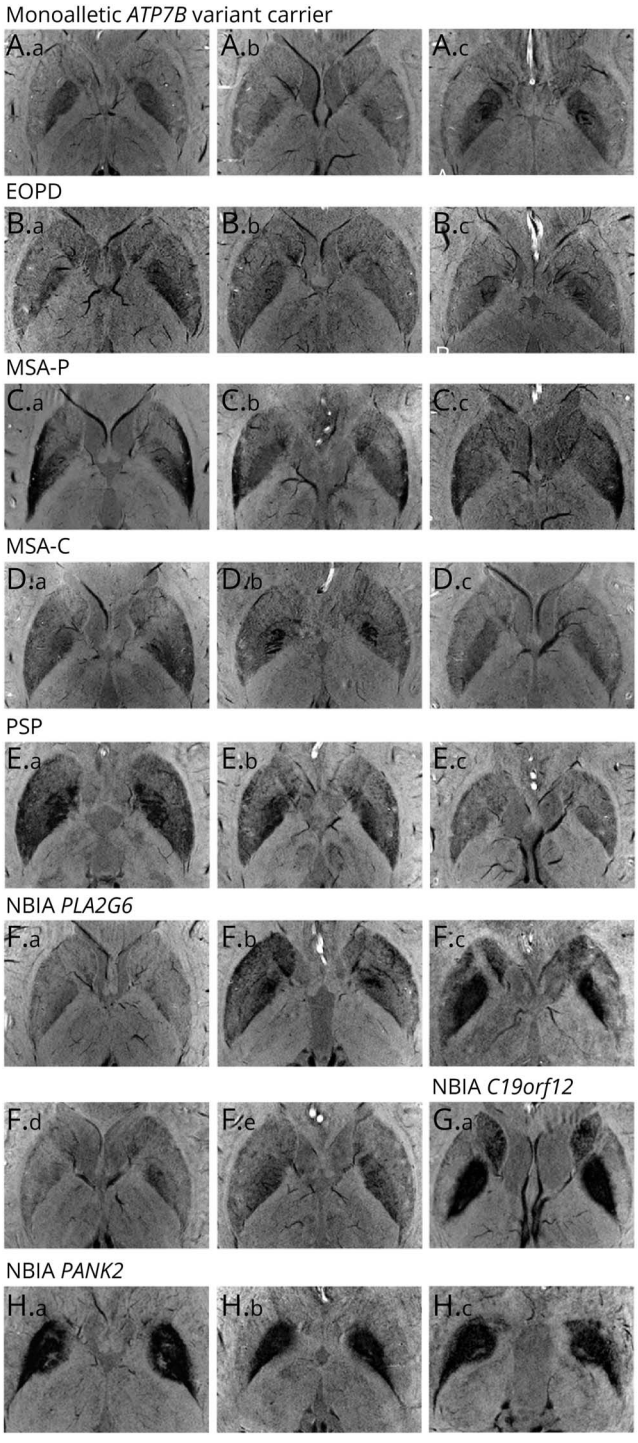

Axial 7T SWI images of the basal ganglia show negative hyperintense globus pallidus rim sign in monoallelic *ATP7B* variant carriers (A.a.-A.c.), EOPD patients (B.a.-B.c.), MSA-P patients (C.a.-C.c.), MSA-C patients (D.a.-D.c.), PSP patients (E.a.-E.c.), and NBIA patients (F.a.-H.c.). EOPD = early-onset Parkinson disease; MSA-C = multiple system atrophy-cerebellar type; MSA-P = multiple system atrophy-parkinsonian type; NBIA = neurodegeneration with brain iron accumulation; PSP = progressive supranuclear palsy; SWI = susceptibility-weighted imaging.

Quantitative Susceptibility Mapping Analysis in the NWD, nNWD, EOPD, MSA-P, MSA-C, PSP, and HC Groups

We compared the QSM values of the globus pallidus and putamen between all patient groups and HC, and between the NWD group and nNWD, EOPD, MSA-P, MSA-C, and PSP groups (Figure 5A, eTable 6). Patients with NWD showed increased susceptibility in the bilateral globus pallidus and putamen compared with nNWD patients, patients with EOPD, and HC, whereas no significant differences in susceptibility in the globus pallidus and putamen were found between nNWD patients and HC. Patients with MSA-P and PSP demonstrated significantly higher susceptibility in the globus pallidus and putamen compared with HC, whereas no significant difference was found among patients with NWD, MSA-P, MSA-C, and PSP.

Principal Component Analysis of QSM in Lenticular Nucleus

In the comparison between patients with NWD and HC, according to the Akaike information criterion (AIC) model, the PC 1 accounted for 64.7% of the variance, which effectively separated between the NWD and HC participants' pattern subject scores, with NWD participants consistently displaying higher subject scores than their HC counterparts ($p < 0.00001$) (eFigure 3A). Patients with NWD demonstrated higher QSM values in the medial putamen and lateral globus pallidus compared with HC. In the comparison between patients with MSA-P and HC, based on the AIC model, the PC 1 accounted for 68.7% of the variance and showed a clear separation between MSA-P and HC participants' pattern subject scores. MSA-P participants consistently had higher subject scores compared with HC participants ($p < 0.00001$) (eFigure 3B). Patients with MSA-P showed higher QSM values in the lateral and caudal putamen compared with HC. In the comparison between patients with MSA-C and HC, based on the AIC model, the PC 1 accounted for 69.5% of the variance, which effectively distinguished between MSA-C and HC participants' pattern subject scores, with MSA-C participants consistently showing higher scores than HC counterparts ($p = 0.00001$) (eFigure 3C). MSA-C participants exhibited higher QSM values in the caudal putamen compared with HC. In the comparison between patients with PSP and HC, according to the AIC model, the PC 1 accounted for 75.8% of the variance, which effectively distinguished between PSP and HC participants' pattern subject scores, with PSP participants consistently showing higher scores than HC counterparts ($p < 0.00001$) (eFigure 3D). PSP participants exhibited higher QSM in the medial and caudal putamen compared with HC. We found no significant differences of pattern scores between nNWD patients and HC and between patients with EOPD and HC ($p = 0.60395$ and $p = 0.75838$, respectively). Of note, the PC 1 varied across different group comparisons, indicating distinct PCs. Voxel-based PCA of QSM values in patients with NWD, MSA-P, MSA-C, and PSP compared with HC, respectively, are shown in Figure 5B. Additional analyses of comparisons

Table 2 Demographic, Clinical, and Imaging Features of the NWD Subgroups

	Active NWD	Stable NWD	*p* Value	Drug-naive NWD	Non–drug-naive NWD	*p* Value
n	22	19	—	10	31	—
Age, y	25.0 (20.8–29.0)	31.0 (21.0–37.0)	0.091[a]	23.0 (19.8–28.8)	29.0 (24.0–36.0)	0.066[a]
Sex, male/female	19/3	11/8	0.04[b]	7/3	23/8	0.795[b]
MMSE	29.0 (28.0–30.0)	29.0 (28.0–30.0)	0.863[a]	29.0 (28.0–30.0)	29.0 (28.0–30.0)	0.589[a]
Disease duration, y	1.4 (0.9–3.0)	10.0 (4.0–15.0)	<0.001[a]	1.3 (0.9–3.0)	5.0 (2.0–13.0)	0.009[a]
Treatment duration of chelating agents and/or zinc salts, y	0.2 (0.0–0.7)	6.0 (3.0–15.0)	<0.001[a]	0.0 (0.0–0.0)	3.0 (0.7–13.0)	<0.001[a]
Treatment						
Chelating agents (D-penicillamine, dimercaptosuccinic acid)	10 (45.5)	17 (89.5)	0.003[b]	0 (0.0)	27 (87.1)	<0.001[b]
Zinc salts	11 (50.0)	15 (78.9)	0.055[b]	0 (0.0)	26 (83.9)	<0.001[b]
GAS for WD	18.0 (13.0–26.0)	11.0 (9.0–13.0)	<0.001[a]	18.5 (14.5–26.8)	12.0 (9.0–17.0)	0.028[a]
UWDRS	36.0 (15.5–46.5)	10.0 (5.0–15.0)	<0.001[a]	33.0 (18.5–50.0)	14.0 (8.0–36.0)	0.031[a]
Kayser-Fleischer ring	21 (95.5)	15 (78.9)	0.107[b]	9 (90.0)	27 (87.1)	0.807[b]
Serum ceruloplasmin, mg/L	32.0 (22.9–48.6)	36.1 (25.9–63.2)	0.553[a]	31.2 (20.5–39.8)	36.0 (26.5–64.9)	0.325[a]
Hyperintense globus pallidus rim sign	22 (100.0)	16 (84.2)	0.053[b]	10 (100.0)	28 (90.3)	0.307[b]
T2/SWI hypointensity	22 (100.0)	18 (94.7)	0.276[b]	10 (100.0)	30 (96.8)	0.565[b]

Abbreviations: GAS for WD = Global Assessment Scale for Wilson disease; MMSE = Mini-Mental State Examination; NWD = neurologic Wilson disease; SWI = susceptibility-weighted imaging; UWDRS = Unified Wilson's Disease Rating Scale.
[a] Mann-Whitney *U* test.
[b] χ^2 test.

between patients with NWD and patients with MSA-P, MSA-C, and PSP can be found in eAppendix 1.

Classification of Evidence

The study provides Class II evidence that the hyperintense globus pallidus rim sign on 7T SWI MRI can accurately diagnose neurologic WD.

Discussion

In this cross-sectional diagnostic study, we identified a distinctive pattern of metal deposition in NWD using 7T SWI, termed "hyperintense globus pallidus rim sign," which demonstrated excellent diagnostic performance. It was observed in 38 of the 41 patients with NWD and was absent in all patients with nNWD, EOPD, MSA, PSP, and NBIA, as well as monoallelic *ATP7B* variant carriers and HC in our study. Moreover, the scoring criteria of the hyperintense globus pallidus rim sign proved useful in monitoring neurologic severity of NWD. QSM and PCA showed excessive metal deposition in the lenticular nucleus with high regional weights in the lateral globus pallidus and medial putamen in patients with NWD, implying a special metal deposition pattern of NWD.

The hyperintense globus pallidus rim sign demonstrated excellent diagnostic sensitivity and specificity (92.7% and 100%, respectively). Although efforts have been made to identify specific imaging characteristics of WD, such as the "face of the giant panda," "miniature panda," "split thalamus," "bright claustrum," and "whorl" signs, these features have been associated with edema, demyelination, gliosis, and brain atrophy, all of which are common among neurodegenerative or metabolic diseases.[8-10] T2/SWI hypointensity was also detected in nNWD, EOPD, MSA, PSP, and NBIA patients, indicating its low diagnostic specificity compared with the hyperintense globus pallidus rim sign. In addition, we found high prevalence of the hyperintense globus pallidus rim sign in drug-naive NWD subgroups, reflecting its high diagnostic efficacy. As brain MRI is used in the current diagnostic process of NWD,[7] the novel hyperintense globus pallidus rim sign can improve the diagnostic accuracy of NWD.

Although WD is inherited in an autosomal recessive manner, between 1% and 39.9% of patients were found with only 1 pathogenic *ATP7B* variant,[37,38] and many novel variants are yet to be discovered.[37] In our study, the hyperintense globus pallidus rim sign was positive in the only 1 NWD patient with monoallelic *ATP7B* variants and was negative in all 22 monoallelic *ATP7B* variant carriers. For individuals with monoallelic *ATP7B* variants, the genetic test alone may be insufficient to make a definitive diagnosis. The hyperintense globus pallidus rim sign can thus assist in the diagnosis of these cases.

Figure 5 Comparison of QSM Values and PCA of QSM in the Lenticular Nucleus

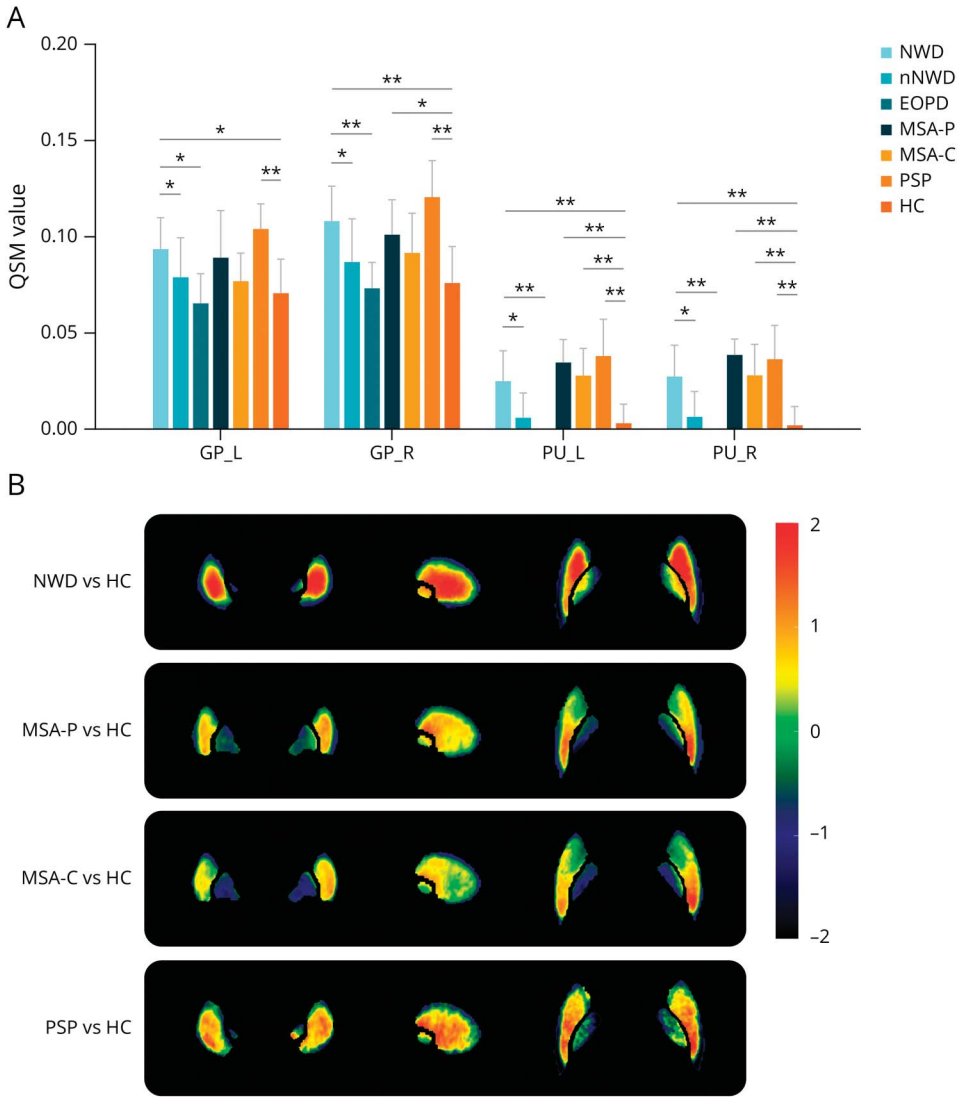

(A) Comparison of QSM values of the NWD, nNWD, EOPD, MSA-P, MSA-C, PSP, and HC groups. (B) Regional weights of the QSM component in the NWD, MSA-P, MSA-C, and PSP groups compared with HC, respectively. The colors represent the region-specific weights on each component. EOPD = early-onset Parkinson disease; GP = globus pallidus; HC = healthy control; L = left; MSA-C = multiple system atrophy-cerebellar type; MSA-P = multiple system atrophy-parkinsonian type; NWD = neurologic Wilson disease; nNWD = nonneurologic Wilson disease; PCA = principal component analysis; PSP = progressive supranuclear palsy; PU = putamen; QSM = quantitative susceptibility mapping; R = right. *$p < 0.05$ and **$p < 0.001$.

We also established a semiquantitative scoring criterion, termed "hyperintense globus pallidus rim sign score," and confirmed its positive correlation with UWDRS scores in patients with NWD. Therefore, apart from its high diagnostic accuracy, the hyperintense globus pallidus rim sign could also be used as a reliable biomarker for the monitoring of neurologic impairment.

Anatomically, the linear hyperintensity at the lateral border of the globus pallidus likely corresponds to the external medullary lamina, which consists of white matter fiber bundles between the globus pallidus and the putamen.[39,40] The presence of the hyperintense globus pallidus rim sign could be related to (1) a pseudohyperintensity change due to contrast of signal intensity between the external medullary lamina and its adjacent structures, i.e., the lenticular nucleus, and (2) hyperintensity change of the external medullary lamina itself due to impairments such as edema or gliosis. However, as the external medullary lamina is a thin structure, with a width of less than 0.6 mm, regional QSM or fiber tracking analysis could not be performed on this particular area. We instead examined the susceptibility change and metal distribution pattern of its adjacent structures.

Increased susceptibility in the globus pallidus and putamen in patients with NWD compared with nNWD patients and HC was observed, with similar results found in previous studies.[41,42] A post mortem 7T MRI and histopathologic study confirmed both copper and iron deposition in the putamen and copper deposition in the globus pallidus of NWD, and established positive correlations between the R2* value and iron (rather than copper) concentrations of the globus pallidus and putamen.[13] Another 9.4 T MRI study reported positive correlations between QSM values and copper concentrations in the primary motor cortex, sensorimotor cortex, amygdaloid nucleus, hippocampus, corpus

striatum, and cerebellum in a mouse model.[43] As these studies had different magnetic fields, species, and brain regions of interest, additional in vitro and in vivo studies on the relationship between imaging and histopathology measurements are required. Nonetheless, both copper and iron deposition should be accounted when interpreting the current QSM results in patients with NWD.

We found lower susceptibility values in the globus pallidus and putamen in patients with EOPD compared with patients with NWD, and no significant differences were found among patients with NWD, MSA-P, MSA-C, and PSP. As the hyperintense globus pallidus rim sign was absent in all nNWD, EOPD, MSA-P, MSA-C, and PSP patients despite altered susceptibility values in our study, it could be hypothesized that the existence of this pseudohyperintensity change may be attributed to 2 mechanisms: (1) excessive metal deposition in the lenticular nucleus revealed by its increased susceptibility values and (2) abnormal metal distribution in a particular region of the lenticular nucleus adjacent to the external medullary lamina, with relatively milder iron deposition in the external medullary lamina. To validate this hypothesis, we performed PCA of QSM values in the lenticular nucleus. A specific metal distribution pattern characterized by excessive metal deposition in the lenticular nucleus with high regional weights in both lateral globus pallidus and medial putamen was established in patients with NWD. By contrast, patients with MSA-P, MSA-C, and PSP demonstrated high regional weights mostly in the caudal putamen and not in the globus pallidus. For the NBIA group, although these patients were not included in the QSM analysis because of limited sample size, we observed hypointensity of the globus pallidus in NBIA patients with *PLA2G6*, *C19orf12*, or *PANK2* variants compared with HC. As discussed in a recent review, while WD, phospholipase A2-associated neurodegeneration (PLAN), mitochondrial membrane protein-associated neurodegeneration (MPAN), and pantothenate kinase-associated neurodegeneration (PKAN) all showed excessive iron deposits in the globus pallidus macroscopically, their microscopic patterns and presumably also pathophysiologic mechanisms of iron deposits were different: for WD, iron was deposited in macrophages and astrocytes; for MPAN and PKAN, in astrocytes, macrophages, and neurons; and for PLAN, in macrophages.[20] Thus, we may conclude that the hyperintense globus pallidus rim sign reflects a pseudohyperintense signal of the external medullary lamina due to excessive metal accumulation in the lenticular nucleus, especially in the lateral globus pallidus and medial putamen, indicating a specific metal distribution pattern in the lenticular nucleus of NWD. However, whether the external medullary lamina itself is involved in the pathophysiologic mechanism of NWD is warranted in further investigation.

Consistent with our observation that the hyperintense globus pallidus rim sign reflected neurologic severity, we found it absent in all nNWD patients, with no significant difference of susceptibility found between nNWD patients and HC. However, other researchers have reported increased susceptibility value in the right globus pallidus of hepatic WD compared with HC and no significant difference between NWD and hepatic WD.[44] This discrepancy could be attributed to the limited number of cases and different definitions and disease stages of the patient subgroups. As nNWD may represent an earlier stage of NWD without neurologic impairment, whether the hyperintense globus pallidus rim sign can be detected in the current cohort of nNWD patients who later develop neurologic symptoms requires validation in further longitudinal study.

For patients with NWD with negative hyperintense globus pallidus rim sign, 2 of the 3 patients received long-term treatment at an early stage of the disease and were experiencing mild clinical symptoms during this study. The third patient, who was also under treatment and had mild neurologic impairment with a UWDRS score of 2, exhibited a trend resembling the hyperintense globus pallidus rim sign with a hypointense signal in the anterior putamen forming a linear hyperintensity less than half of the lateral border of the globus pallidus. A previous study has demonstrated both imaging (measured by corrected phase values of the putamen and globus pallidus) and clinical (assessed by the modified Young scale) recovery after metal chelating treatment,[15] which may influence the appearance of the hyperintense globus pallidus rim sign. As the hyperintense globus pallidus rim sign was observed in all drug-naive patients with NWD, it could have higher diagnostic accuracy in drug-naive NWD. Further longitudinal studies will be essential to examine the treatment effect on this feature.

Several limitations should be noted. First, as a cross-sectional study, alterations of the hyperintense globus pallidus rim sign in patients with NWD due to treatment effect and in nNWD patients who later develop neurologic symptoms require further verification in cohort studies. Second, confined by the current analysis approach, regional susceptibility and fiber analysis could not be performed on the linear hyperintensity signal area. As well, the number of asymptomatic patient with WD identified through family screening was small (3 in this study), and future studies will require larger patient population. Imaging characteristics of patient subgroups with pure psychiatric symptoms and with liver failure also deserve particular emphasis. Finally, as a single-center study, our imaging protocols require validation in multicenter studies using different MRI scanners and sequence parameters. More research on the contraindications of 7T MRI in human studies is warranted. Meanwhile, despite the increased utilization of 7T systems in the past decade, its availability is still rather limited compared with scanners of lower magnetic field intensities such as 1.5 and 3 T. Thus, investigations of the presence of the hyperintense globus pallidus rim sign at lower magnetic field intensities are needed.

In conclusion, our study identified a distinctive pattern of metal deposition, termed the "hyperintense globus pallidus rim sign," which may serve as an effective neuroimaging biomarker for the diagnosis, differential diagnosis, and

monitoring of the neurologic impairment of NWD using SWI at 7T. It revealed a unique pattern of metal deposition in the lenticular nucleus of patients with NWD. Further pathologic studies are warranted to elucidate the pathogenetic mechanisms of our findings.

Acknowledgment

The authors acknowledge the support of the participants and their families for taking part in the study. The authors thank all research staff at the four participating sites and Dr. Michael L. Schilsky for revision of the manuscript. Their dedication made the study feasible.

Study Funding

This work was supported by the National Natural Science Foundation of China (No. 82271459 and No. 82071422) and Natural Science Foundation of Beijing Municipality (No. 7212031).

Disclosure

The authors report no relevant disclosures. Go to Neurology.org/N for full disclosures.

Publication History

Received by *Neurology* November 20, 2023. Accepted in final form March 11, 2024. Submitted and externally peer reviewed. The handling editor was Associate Editor Peter Hedera, MD, PhD.

Appendix Authors

Name	Location	Contribution
Dongning Su, MD, PhD	Department of Neurology, Beijing Tiantan Hospital, Capital Medical University; China National Clinical Research Center for Neurologic Diseases, Beijing, China	Drafting/revision of the manuscript for content, including medical writing for content; major role in the acquisition of data; study concept or design; analysis or interpretation of data
Zhijin Zhang, BS	Department of Neurology, Beijing Tiantan Hospital, Capital Medical University; China National Clinical Research Center for Neurologic Diseases, Beijing, China	Drafting/revision of the manuscript for content, including medical writing for content; major role in the acquisition of data; study concept or design; analysis or interpretation of data
Zhe Zhang, PhD	China National Clinical Research Center for Neurologic Diseases, Beijing; Tiantan Neuroimaging Center of Excellence, Beijing Tiantan Hospital, Capital Medical University, China	Drafting/revision of the manuscript for content, including medical writing for content; major role in the acquisition of data; study concept or design; analysis or interpretation of data
Sujun Zheng, MD, PhD	Department of Hepatology, Beijing Youan Hospital, Capital Medical University, Beijing, China	Major role in the acquisition of data
Tingyan Yao, BS	Department of Neurology, Xuanwu Hospital, Capital Medical University, National Clinical Research Center for Geriatric Disorders, Beijing, China	Major role in the acquisition of data
Yi Dong, MD, PhD	Senior Department of Hepatology, the Fifth Medical Center of PLA General Hospital, Beijing, China	Major role in the acquisition of data
Wanlin Zhu, PhD	China National Clinical Research Center for Neurologic Diseases, Beijing; Tiantan Neuroimaging Center of Excellence, Beijing Tiantan Hospital, Capital Medical University, China	Major role in the acquisition of data
Ning Wei, PhD	China National Clinical Research Center for Neurologic Diseases, Beijing; Tiantan Neuroimaging Center of Excellence, Beijing Tiantan Hospital, Capital Medical University, China	Major role in the acquisition of data
Yue Suo, MD, PhD	China National Clinical Research Center for Neurologic Diseases, Beijing; Tiantan Neuroimaging Center of Excellence, Beijing Tiantan Hospital, Capital Medical University, China	Major role in the acquisition of data
Xinyao Liu, BS	China National Clinical Research Center for Neurologic Diseases, Beijing; Tiantan Neuroimaging Center of Excellence, Beijing Tiantan Hospital, Capital Medical University, China	Major role in the acquisition of data
Huiqing Zhao, MD, PhD	Department of Neurology, Beijing Tiantan Hospital, Capital Medical University; China National Clinical Research Center for Neurologic Diseases, Beijing, China	Major role in the acquisition of data
Zhan Wang, MD, PhD	Department of Neurology, Beijing Tiantan Hospital, Capital Medical University; China National Clinical Research Center for Neurologic Diseases, Beijing, China	Major role in the acquisition of data
Huizi Ma, MD, PhD	Department of Neurology, Beijing Tiantan Hospital, Capital Medical University; China National Clinical Research Center for Neurologic Diseases, Beijing, China	Major role in the acquisition of data
Wei Li, MD, PhD	Department of Neurology, Beijing Tiantan Hospital, Capital Medical University; China National Clinical Research Center for Neurologic Diseases, Beijing, China	Major role in the acquisition of data
Junhong Zhou, PhD	Hinda and Arthur Marcus Institute for Aging Research, Hebrew SeniorLife, Roslindale; Harvard Medical School, Boston, MA	Drafting/revision of the manuscript for content, including medical writing for content; analysis or interpretation of data

Appendix *(continued)*

Name	Location	Contribution
Joyce S.T. Lam, MSc	Pacific Parkinson's Research Centre, Djavad Mowafaghian Centre for Brain Health, University of British Columbia, Vancouver, Canada	Drafting/revision of the manuscript for content, including medical writing for content
Tao Wu, MD, PhD	Department of Neurology, Beijing Tiantan Hospital, Capital Medical University; China National Clinical Research Center for Neurologic Diseases, Beijing, China	Drafting/revision of the manuscript for content, including medical writing for content; analysis or interpretation of data
Petr Dusek, MD	Department of Neurology and Centre of Clinical Neuroscience, First Faculty of Medicine, Charles University and General University Hospital, Prague, Czech Republic	Drafting/revision of the manuscript for content, including medical writing for content; analysis or interpretation of data
A. Jon Stoessl, MD	Pacific Parkinson's Research Centre, Djavad Mowafaghian Centre for Brain Health, and Division of Neurology, Department of Medicine, University of British Columbia, Vancouver, Canada	Drafting/revision of the manuscript for content, including medical writing for content; analysis or interpretation of data
Xiaoping Wang, MD, PhD	Department of Neurology, Jiading Branch of Shanghai General Hospital, Shanghai Jiao Tong University School of Medicine, China	Drafting/revision of the manuscript for content, including medical writing for content; study concept or design; analysis or interpretation of data
Jing Jing, MD, PhD	Department of Neurology, Beijing Tiantan Hospital, Capital Medical University; China National Clinical Research Center for Neurologic Diseases; Tiantan Neuroimaging Center of Excellence, Beijing Tiantan Hospital, Capital Medical University, China	Drafting/revision of the manuscript for content, including medical writing for content; major role in the acquisition of data; study concept or design; analysis or interpretation of data
Tao Feng, MD, PhD	Department of Neurology, Beijing Tiantan Hospital, Capital Medical University; China National Clinical Research Center for Neurologic Diseases, Beijing, China	Drafting/revision of the manuscript for content, including medical writing for content; major role in the acquisition of data; study concept or design; analysis or interpretation of data

References

1. Czlonkowska A, Litwin T, Dusek P, et al. Wilson disease. *Nat Rev Dis Primers*. 2018;4(1):21. doi:10.1038/s41572-018-0018-3
2. Ferenci P, Caca K, Loudianos G, et al. Diagnosis and phenotypic classification of Wilson disease. *Liver Int*. 2003;23(3):139-142. doi:10.1034/j.1600-0676.2003.00824.x
3. Walter U, Krolikowski K, Tarnacka B, Benecke R, Czlonkowska A, Dressler D. Sonographic detection of basal ganglia lesions in asymptomatic and symptomatic Wilson disease. *Neurology*. 2005;64(10):1726-1732. doi:10.1212/01.WNL.0000161847.46465.B9
4. Shribman S, Poujois A, Bandmann O, Czlonkowska A, Warner TT. Wilson's disease: update on pathogenesis, biomarkers and treatments. *J Neurol Neurosurg Psychiatry*. 2021;92(10):1053-1061. doi:10.1136/jnnp-2021-326123
5. Beinhardt S, Leiss W, Stättermayer AF, et al. Long-term outcomes of patients with Wilson disease in a large Austrian cohort. *Clin Gastroenterol Hepatol*. 2014;12(4):683-689. doi:10.1016/j.cgh.2013.09.025
6. Merle U, Schaefer M, Ferenci P, Stremmel W. Clinical presentation, diagnosis and long-term outcome of Wilson's disease: a cohort study. *Gut*. 2007;56(1):115-120. doi:10.1136/gut.2005.087262
7. European Association for Study of Liver. EASL clinical practice guidelines: Wilson's disease. *J Hepatol*. 2012;56(3):671-685. doi:10.1016/j.jhep.2011.11.007
8. Zhong W, Huang Z, Tang X. A study of brain MRI characteristics and clinical features in 76 cases of Wilson's disease. *J Clin Neurosci*. 2019;59:167-174. doi:10.1016/j.jocn.2018.10.096
9. Prashanth L, Sinha S, Taly A, Vasudev M. Do MRI features distinguish Wilson's disease from other early onset extrapyramidal disorders? An analysis of 100 cases. *Mov Disord*. 2010;25(6):672-678. doi:10.1002/mds.22689
10. Rędzia-Ogrodnik B, Członkowska A, Antos A, et al. Pathognomonic neuroradiological signs in Wilson's disease: truth or myth? *Parkinsonism Relat Disord*. 2023;107:105247. doi:10.1016/j.parkreldis.2022.105247
11. Lallas M, Desai J. Wernicke encephalopathy in children and adolescents. *World J Pediatr*. 2014;10(4):293-298. doi:10.1007/s12519-014-0506-9
12. Das SK, Ray K. Wilson's disease: an update. *Nat Clin Pract Neurol*. 2006;2(9):482-493. doi:10.1038/ncpneuro0291
13. Dusek P, Bahn E, Litwin T, et al. Brain iron accumulation in Wilson disease: a post mortem 7 Tesla MRI: histopathological study. *Neuropathol Appl Neurobiol*. 2017;43(6):514-532. doi:10.1111/nan.12341
14. Litwin T, Gromadzka G, Szpak G, Jabłonka-Salach K, Bulska E, Członkowska A. Brain metal accumulation in Wilson's disease. *J Neurol Sci*. 2013;329(1-2):55-58. doi:10.1016/j.jns.2013.03.021
15. Zhou X, Xiao X, Li XH, et al. A study of susceptibility-weighted imaging in patients with Wilson disease during the treatment of metal chelator. *J Neurol*. 2020;267(6):1643-1650. doi:10.1007/s00415-020-09746-y
16. Li G, Wu R, Tong R, et al. Quantitative measurement of metal accumulation in brain of patients with Wilson's disease. *Mov Disord*. 2020;35(10):1787-1795. doi:10.1002/mds.28141
17. Dusek P, Lescinskij A, Ruzicka F, et al. Associations of brain atrophy and cerebral iron accumulation at MRI with clinical severity in Wilson disease. *Radiology*. 2021;299(3):662-672. doi:10.1148/radiol.2021202846
18. Su D, Zhang Z, Zhang Z, et al. Microstructural and functional impairment of the basal ganglia in Wilson's disease: a multimodal neuroimaging study. *Front Neurosci*. 2023;17:1146644. doi:10.3389/fnins.2023.1146644
19. Yuan XZ, Li GY, Chen JL, Li JQ, Wang XP. Paramagnetic metal accumulation in the deep gray matter nuclei is associated with neurodegeneration in Wilson's disease. *Front Neurosci*. 2020;14:573633. doi:10.3389/fnins.2020.573633
20. Dusek P, Hofer T, Alexander J, Roos PM, Aaseth JO. Cerebral iron deposition in neurodegeneration. *Biomolecules*. 2022;12(5):714. doi:10.3390/biom12050714.
21. Cong F, Liu X, Liu C, et al. Improved depiction of subthalamic nucleus and globus pallidus internus with optimized high-resolution quantitative susceptibility mapping at 7 T. *NMR Biomed*. 2020;33(11):e4382. doi:10.1002/nbm.4382
22. Yao B, Li T, Gelderen P, Shmueli K, de Zwart J, Duyn J. Susceptibility contrast in high field MRI of human brain as a function of tissue iron content. *Neuroimage*. 2009;44(4):1259-1266. doi:10.1016/j.neuroimage.2008.10.029
23. Blazejewska AI, Schwarz ST, Pitiot A, et al. Visualization of nigrosome 1 and its loss in PD: pathoanatomical correlation and in vivo 7 T MRI. *Neurology*. 2013;81(6):534-540. doi:10.1212/WNL.0b013e31829e6fd2
24. Dal-Bianco A, Grabner G, Kronnerwetter C, et al. Long-term evolution of multiple sclerosis iron rim lesions in 7 T MRI. *Brain*. 2021;144(3):833-847. doi:10.1093/brain/awaa436
25. Schrag A, Schott JM. Epidemiological, clinical, and genetic characteristics of early-onset parkinsonism. *Lancet Neurol*. 2006;5(4):355-363. doi:10.1016/S1474-4422(06)70411-2
26. Ravanfar P, Loi S, Syeda W, et al. Systematic review: quantitative susceptibility mapping (QSM) of brain iron profile in neurodegenerative diseases. *Front Neurosci*. 2021;15:618435. doi:10.3389/fnins.2021.618435
27. Levi S, Tiranti V. Neurodegeneration with brain iron accumulation disorders: valuable models aimed at understanding the pathogenesis of iron deposition. *Pharmaceuticals (Basel)*. 2019;12(1):27. doi:10.3390/ph12010027
28. Postuma RB, Berg D, Stern M, et al. MDS clinical diagnostic criteria for Parkinson's disease. *Mov Disord*. 2015;30(12):1591-1601. doi:10.1002/mds.26424
29. Gilman S, Wenning GK, Low PA, et al. Second consensus statement on the diagnosis of multiple system atrophy. *Neurology*. 2008;71(9):670-676. doi:10.1212/01.wnl.0000324625.00404.15
30. Hoglinger GU, Respondek G, Stamelou M, et al. Clinical diagnosis of progressive supranuclear palsy: the movement disorder society criteria. *Mov Disord*. 2017;32(6):853-864. doi:10.1002/mds.26987
31. Shribman S, Bocchetta M, Sudre CH, et al. Neuroimaging correlates of brain injury in Wilson's disease: a multimodal, whole-brain MRI study. *Brain*. 2022;145(1):263-275. doi:10.1093/brain/awab274
32. Aggarwal A, Aggarwal N, Nagral A, Jankharia G, Bhatt M. A novel global assessment scale for Wilson's disease (GAS for WD). *Mov Disord*. 2009;24(4):509-518. doi:10.1002/mds.22231
33. Członkowska A, Tarnacka B, Möller J, et al. Unified Wilson's Disease Rating Scale: a proposal for the neurological scoring of Wilson's disease patients. *Neurol Neurochir Pol*. 2007;41:1-12.
34. Dusek P, Smolinski L, Redzia-Ogrodnik B, et al. Semiquantitative scale for assessing brain MRI abnormalities in Wilson disease: a validation study. *Mov Disord*. 2020;35(6):994-1001. doi:10.1002/mds.28018
35. Acosta-Cabronero J, Milovic C, Mattern H, Tejos C, Speck O, Callaghan MF. A robust multi-scale approach to quantitative susceptibility mapping. *Neuroimage*. 2018;183:7-24. doi:10.1016/j.neuroimage.2018.07.065
36. Burgetova R, Dusek P, Burgetova A, et al. Age-related magnetic susceptibility changes in deep grey matter and cerebral cortex of normal young and middle-aged adults

depicted by whole brain analysis. *Quant Imaging Med Surg*. 2021;11(9):3906-3919. doi:10.21037/qims-21-87
37. Coffey AJ, Durkie M, Hague S, et al. A genetic study of Wilson's disease in the United Kingdom. *Brain*. 2013;136(pt 5):1476-1487. doi:10.1093/brain/awt035
38. Cheng N, Wang H, Wu W, et al. Spectrum of ATP7B mutations and genotype-phenotype correlation in large-scale Chinese patients with Wilson Disease. *Clin Genet*. 2017;92(1):69-79. doi:10.1111/cge.12951
39. Hoch MJ, Bruno MT, Faustin A, et al. 3T MRI whole-brain microscopy discrimination of subcortical anatomy, part 2: basal forebrain. *AJNR Am J Neuroradiol*. 2019; 40(7):1095-1105. doi:10.3174/ajnr.A6088
40. De Barros A, Arribarat G, Lotterie J, Dominguez G, Chaynes P, Péran P. Iron distribution in the lentiform nucleus: a post-mortem MRI and histology study. *Brain Struct Funct*. 2021;226(2):351-364. doi:10.1007/s00429-020-02175-7
41. Dezortova M, Lescinskij A, Dusek P, et al. Multiparametric quantitative brain MRI in neurological and hepatic forms of Wilson's disease. *J Magn Reson Imaging*. 2020; 51(6):1829-1835. doi:10.1002/jmri.26984
42. Jing X-Z, Yuan X-Z, Li G-Y, et al. Increased magnetic susceptibility in the deep gray matter nuclei of Wilson's disease: have we been ignoring atrophy? *Front Neurosci*. 2022;16:794375. doi:10.3389/fnins.2022.794375
43. Han Y, Dong J, Xu C, et al. Application of 9.4T MRI in Wilson disease model TX mice with quantitative susceptibility mapping to assess copper distribution. *Front Behav Neurosci*. 2020;14:59. doi:10.3389/fnbeh.2020.00059
44. Fritzsch D, Reiss-Zimmermann M, Trampel R, Turner R, Hoffmann K, Schäfer A. Seven-tesla magnetic resonance imaging in Wilson disease using quantitative susceptibility mapping for measurement of copper accumulation. *Invest Radiol*. 2014; 49(5):299-306. doi:10.1097/RLI.0000000000000010